FFEMS Fatigue & Fracture of Engineering Materials & Structures

doi: 10.1111/ffe.12189

Multiscale fatigue crack growth modelling for welded stiffened panels

Ž. BOŽIĆ[1], S. SCHMAUDER[2], M. MLIKOTA[2] and M. HUMMEL[2]

[1]*Faculty of Mechanical Engineering and Naval Architecture, University of Zagreb, I. Lučića, 10000 Zagreb, Croatia,* [2]*IMWF, University of Stuttgart, Pfaffenwaldring 32, 70569 Stuttgart, Germany*

Received Date: 27 September 2013; Accepted Date: 9 March 2014; Published Online: 2014

ABSTRACT The influence of welding residual stresses in stiffened panels on effective stress intensity factor (SIF) values and fatigue crack growth rate is studied in this paper. Interpretation of relevant effects on different length scales such as dislocation appearance and microstructural crack nucleation and propagation is taken into account using molecular dynamics simulations as well as a Tanaka–Mura approach for the analysis of the problem. Mode I SIFs, K_I, were calculated by the finite element method using shell elements and the crack tip displacement extrapolation technique. The total SIF value, K_{tot}, is derived by a part due to the applied load, K_{appl}, and by a part due to welding residual stresses, K_{res}. Fatigue crack propagation simulations based on power law models showed that high tensile residual stresses in the vicinity of a stiffener significantly increase the crack growth rate, which is in good agreement with experimental results.

Keywords dislocation; fatigue crack growth rate; microstructurally small cracks; residual stress.

NOMENCLATURE

a	=	half crack length
a_0	=	initial crack length
a_{fin}	=	final crack length
C	=	material constant of the Paris equation
CRSS	=	critical resolved shear stress
d	=	slip band length
$\mathrm{d}a/\mathrm{d}N$	=	crack growth rate
E	=	Young's modulus
$F(\vec{r},t)$	=	interatomic force
F_{max}	=	maximum applied force
F_{min}	=	minimum applied force
G	=	shear modulus
K	=	stress intensity factor (SIF)
K_{appl}	=	stress intensity factor due to the applied load
K_{res}	=	stress intensity factor due to weld residual stresses
K_{th}	=	stress intensity factor threshold
K_{tot}	=	total stress intensity factor
m	=	atomic mass
m	=	material constant of the Paris equation
N	=	number of stress cycles for the fatigue crack propagation
N_f	=	number of stress cycles for fatigue failure
N_g	=	number of stress cycles required for crack nucleation in a single grain
N_{ini}	=	number of stress cycles needed for the initiation of a small crack
R	=	stress ratio
R_{eff}	=	effective stress intensity factor ratio
$U(\vec{r},t)$	=	interatomic embedded atom method pair potential
W_c	=	specific fracture energy per unit area

Correspondence: Ž. Božić. E-mail: zeljko.bozic@fsb.hr

ΔF = applied force range
ΔK = stress intensity factor range
ΔK_{eff} = effective stress intensity factor range
$\Delta\sigma$ = average applied stress range
$\Delta\bar{\tau}$ = average shear stress range on the slip band
σ_0 = yield stress

INTRODUCTION

Structural health monitoring and damage detection in aircraft, ship, and offshore and other structures are highly important for their fitness for service assessment. Under cyclic loading, fatigue cracks may initiate at sites of stress concentration and further propagate, which can eventually result in unstable fracture and structural failure. In aircraft, ships and other thin-walled structures stiffened panels are widely used owing to their light weight and high strength and stiffness. Welded stiffened panels are mostly implemented in the deck and side structure of a ship. The crack growth rate in welded stiffened panels can be significantly affected by the residual stresses that are introduced by the welding process. The high heat input from the welding process causes tensile residual stresses in the vicinity of a stiffener. These tensile stresses are equilibrated by compressive stresses in the region between the stiffeners. Residual stresses should be taken into account for a proper fatigue life assessment of welded stiffened panels under cyclic tension loading.

From a physics point of view, the fatigue phenomenon involves multiple length scales due to the presence of microcracks or inclusions that are small compared with the large size of structural components. Therefore, it is necessary to consider the fatigue process at all scales. A scale-dependent physics-based model is required for accurate simulation and understanding of material behaviour in various operational environments to assess fatigue life of a structure.[1–5]

The process of fatigue failure of mechanical components may be divided into the following stages: (1) crack nucleation, (2) small crack growth, (3) long crack growth and (4) occurrence of final failure. In engineering applications, the first two stages are usually termed as the 'crack initiation or small crack formation period' while long crack growth is termed as the 'crack propagation period'.

In pure metals and some alloys without pores or inclusions, irreversible dislocations glide under cyclic loading. This leads to the development of persistent slip bands, extrusions and intrusions in surface grains that are optimally oriented for slip. Dislocation development can be simulated by using the molecular dynamics (MD) simulation code IMD.[6] To analyse dislocation development, atomistic scale simulation methods are implemented.[7–10] With continued strain cycling, a fatigue crack can be nucleated at an extrusion or intrusion within a persistent slip band.[11–18] Non-metallic inclusions, which are present in commercial materials as a result of the production process, can also act as potential sites for fatigue crack nucleation. In the high-cycle regime, fatigue cracks initiate from inclusions and defects on the surface of a specimen or component. For very high-cycle fatigue, fatigue cracks initiate from defects located under the surface of the specimen.[19,20] Microcrack nucleation can be analysed by using the Tanaka–Mura model or some of its modifications.[11,21–24]

Fatigue crack growth prediction models based on fracture mechanics have been developed to support the damage tolerance concepts in metallic structures.[25] A well-known method for predicting fatigue crack propagation under constant stress range is the power law described by Paris and Erdogan.[26] Dexter *et al.*[27] and Mahmoud and Dexter[28] analysed the growth of long fatigue cracks in stiffened panels and simulated the crack propagation in box girders with welded stiffeners. They conducted cyclic tension fatigue tests on approximately half-scale welded stiffened panels to study propagation of large cracks as they interact with the stiffeners. Measured welding residual stresses were introduced in the finite element (FE) model, and crack propagation life was simulated. Sumi *et al.*[29] studied the fatigue growth of long cracks in stiffened panels of a ship deck structure under cyclic tension loading. For that purpose, fatigue tests were carried out on welded stiffened panel specimens damaged with a single crack or an array of collinear cracks.

In order to analyse the total fatigue life of a structural component or a test specimen, from crack initiation through cyclic slip mechanism up to long crack propagation and final failure, a multiscale approach is needed. Figure 1 shows a schematic description of bridging between the three considered scales: nanoscale, microscale and macroscale. The relevant material's property parameter from atomistic scale needed for the micromechanics modelling is the critical resolved shear stress (CRSS). The CRSS is inferred from MD simulation, and it is the input parameter for a modified Tanaka–Mura model. The modified Tanaka–Mura micromechanics model provides information on the number of loading cycles to initiate a small crack and its size. This information is further an input for the macroscale fatigue crack growth

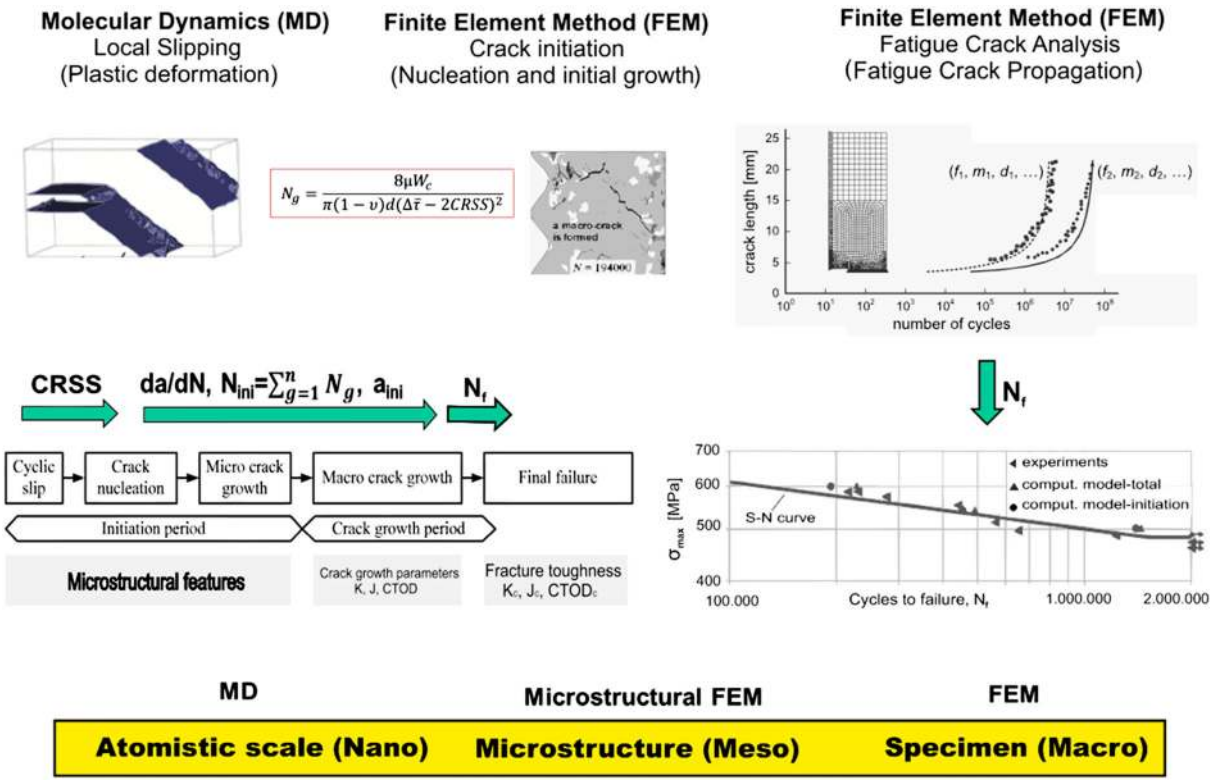

Fig. 1 A schematic description of bridging between the three considered scales.

model based on power law equations, by means of which then a total fatigue life up to fracture as a final event can be assessed. Based on the presented procedure, the fatigue behaviour of a material can be simulated, and new materials can be modelled and analysed. In this way, Wöhler curves can be obtained for new materials without experiments.

This paper presents a study of the influence of welding residual stresses in stiffened panels on effective stress intensity factor (SIF) values and fatigue crack growth rate. A total SIF value, K_{tot}, was obtained by a linear superposition of the SIF values due to the applied load, K_{appl}, and due to weld residual stresses, K_{res}. The effective SIF value, K_{eff}, was considered as a crack growth driving force in a power law model.[30,31] Mode I SIF values, K_I, were calculated by the FE software package ANSYS using shell elements and the crack tip displacement extrapolation method in an automatic post-processing procedure.[32] Simulated fatigue crack propagation life was compared with the experimental results as obtained by Sumi *et al.*[29] The MD simulation was implemented to analyse dislocation development in an iron cuboid model with a triangular notch tip. Numerical simulations of the fatigue crack initiation and growth for martensitic steel, based on modified Tanaka–Mura model, were carried out.

MOLECULAR DYNAMICS SIMULATION OF DISLOCATION DEVELOPMENT IN IRON

Methods and model

Taking a close look on dislocation development leads to the necessity of atomistic scale simulation methods. Therefore, we used for the present work the MD simulation code IMD.[6] It was developed at the Institute of Theoretical and Applied Physics belonging to the University of Stuttgart. In MD, the atoms are seen as mass m points at the position $\vec{r}$ for which the elementary Newton's equations of motion

$$F(\vec{r}, t) = m * \frac{\partial^2 \vec{r}}{\partial^2 t} \tag{1}$$

are solved in every time step. The force $F(\vec{r}, t)$ is given by the derivative of the interatomic embedded atom method[7] pair potential $U(\vec{r}, t)$ (2):

$$F(\vec{r}, t) = -\nabla U(\vec{r}, t). \tag{2}$$

The system we investigated contains about half a million iron atoms (Fig. 2). They form a cuboid of the size $286 \times 143 \times 143$ Å^3 where a notch (dimension 15×90 Å^2) with a triangular notch tip was inserted along the (110) plane.

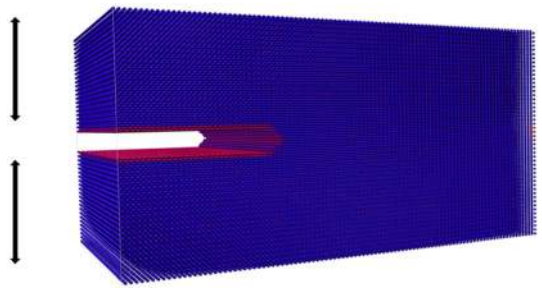

Fig. 2 Body centred crystal iron cuboid $286 \times 143 \times 143\,\text{Å}^3$ with a $15 \times 90\,\text{Å}^2$ notch on a (110) plane. The 486 000 atoms are colour coded via von Mises stress (red indicates high stress and blue low stress). Image by MegaMol™.[8] Full periodic boundary conditions are applied. The loading direction is marked by the arrows.

Cyclic deformation of the simulation box was applied in the [001]-direction. Therefore, the z-component of the simulation cell was elongated with a constant rate of 5×10^{-7} at each time step. The value 5×10^{-7} represents a factor by which z-components of the system are multiplied at each time step; therefore, it is without units. The strain rate could be calculated as $2.5 \times 10^{8}\,\text{s}^{-1}$. Such high strain rates are typical for MD simulations but very high for experimentalists. After reaching a strain of 7%, we applied pressure at the same rate until we reach 7% of strain in compression. Seven percent tends to be at the upper end of the elastic elongation regime. In order to reduce computation time and still observe changes in the structure already in the very first cycles, one has to apply these high values of maximum strain. Still, this value should be realistic. For that reason, the authors used an input strain value of 7%. There have been other simulations with lower maximum strain, where the formation of dislocations occurs after a higher number of cycles. The loading and unloading was repeated continuously. The temperature was chosen to be room temperature (300 K). The time step was fixed to 2 fs. Periodic boundary conditions were used in every direction.

Results and discussion

During the continuous cyclic change from elongation to compression, different stages of the system appeared (Fig. 3).

- Stage I: Configuration under no pressure.
- Stage II: Initiation of reversible local restructuring under tensile loading.
- Stage III: Formation of one continuous plane with face centred cubic (fcc) structure.
- Stage IV: Compression leads to a resolution of the deformation introduced in the previous steps into the structure and to bending of the middle of the notch surfaces towards each other up to a minimum distance of 6.8 Å.
- Stage V: During the fourth loading cycle, dislocations are initiated. The dislocation extraction algorithm[9] detects 'defect surfaces'. 'The defect surface consists of

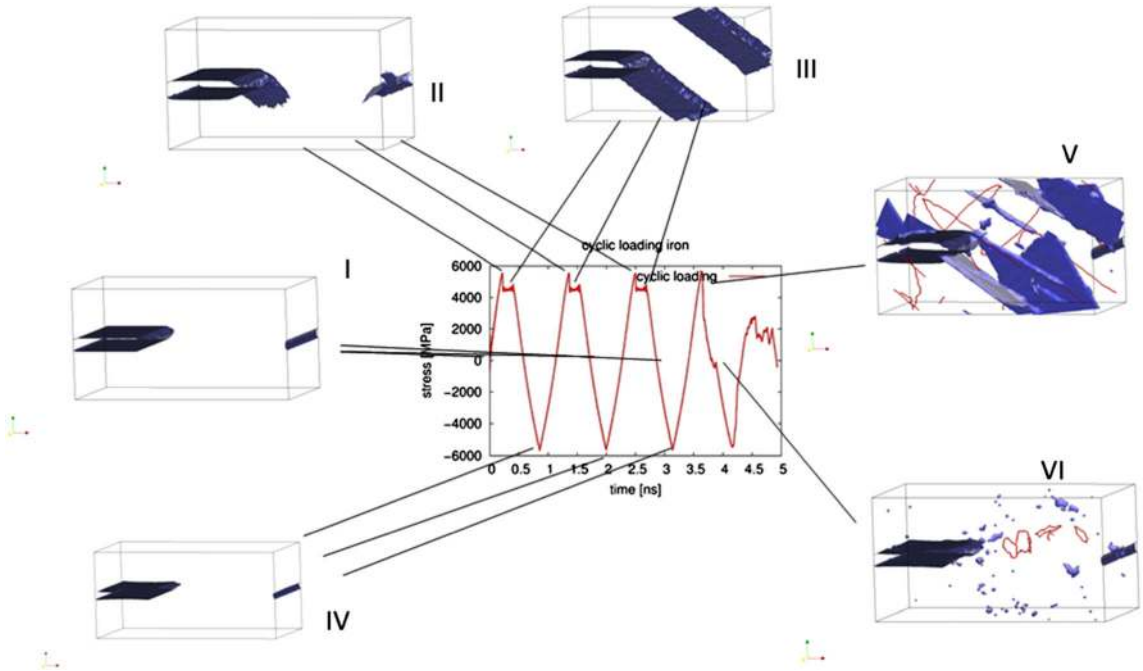

Fig. 3 Stress (MPa) in z-direction in terms of the time (ns) during cyclic loading of a nanostructure of a notched iron cuboid. System configurations at different times are depicted: blue are according to dislocation extraction algorithm[9] 'defect surfaces', and red represents dislocations. The view is from lower left.

those parts of the interface mesh, which have not been swept by elastic Burgers circuits.'[10]
- Stage VI: Dislocations still remain in the structure even though no pressure remains in the system.

The MD simulations presented here illustrate the development of the system from reversible plastic deformation to irreversible plastic deformation including dislocation nucleation, propagation, backpropagation and multiplication. The quite high stress level of the system in the regime of 5.5 GPa during dislocation nucleation is attributed to the fact that the underlying model is assumed to be an internally defect-free single crystal, except for the external notch, and to a minor degree to the high strain rate that is applied in this simulation. Strain rate effects in MD simulations have been previously discussed in literature, for example,[33] and will thus not be taken into further account here. The stress to propagate an artificially introduced dislocation in an MD model is frequently obtained via pure shear simulations in literature[34] and at the IMWF as demonstrated, for example, by Kohler *et al.*[35] At 10 K Kumar *et al.*[36] obtained a value of 81 MPa with the FeCFe potential presented by Bonny *et al.*[7] which is in close agreement with about 84 MPa which we have found in our group for 0 K.

In the presented simulations here, the intention was to force dislocation nucleation and to study such naturally formed dislocations as a realistic basis for dislocation movement analyses rather than to use artificially implanted dislocations in the model. In the first two peaks, a reversible body centred crystal–fcc Bain transition from α-Fe to γ-Fe takes place (stage III, Fig. 3). The oscillation of the stress–time curve (stage III, Fig. 3) is explained by the formation of stacking faults inside the transition fcc phase. In contrast to Farkas *et al.*,[37] where it was believed that the emission of Shockley partial dislocations is relevant for the stacking fault formation, no dislocations are observed in our simulation at this early stage.

Dislocation nucleation takes place as the irreversible deformation begins. The small spikes in the stress–time curve are identified as single dislocation movement. The height of the spike, which is related to the CRSS to move a dislocation, is calculated to a value of 293 MPa, taking into account that this value is higher than the CRSS because of the angle of the dislocations glide plane with respect to the loading axis and the, thus, involved Schmid factor that amounts to 0.40 in the present case: The CRSS value obtained from the present simulation is calculated according to Schmid's law to be $\tau = 293\,\text{MPa} \cos 26.5° \cos 63.5° = 117\,\text{MPa}$, which is in very good agreement to pure shear simulations mentioned earlier[36] and to an even better degree with an experimental value of 108 MPa, which has been previously used for microscale modelling of fatigue by Jezernik *et al.*[24] for the present material.

MICROSTRUCTURAL CRACK NUCLEATION AND PROPAGATION

To solve problems of crack nucleation, the Tanaka–Mura model[11,21–24] is frequently used. In the two articles,[21,22] Tanaka and Mura proposed dislocation models for treating fatigue crack nucleation at slip bands. Tanaka and Mura envisioned that fatigue crack nucleation occurs by the accumulation of dislocation dipoles in a single grain during strain cycling. In the theory of fatigue crack nucleation in slip bands, the forward and reverse plastic flows within slip bands are caused by dislocations with different signs moving on two closely located layers. It is assumed that their movements are irreversible. Based on the Tanaka–Mura model, the monotonic build-up of dislocation dipoles is systematically derived from the theory of continuously distributed dislocations. The number of stress cycles up to the nucleation of a crack about one grain diameter in length is reached when the self-strain energy of the accumulated dislocation dipoles reaches a critical value. The number of stress cycles N_g required for crack nucleation in a single grain can be determined as follows:

$$N_g = \frac{8GW_c}{\pi(1-\nu)d(\Delta\bar{\tau} - 2CRSS)^2}. \tag{3}$$

Equation (3) presumes that cracks form along slip bands within grains, depending on slip band length d and average shear stress range $\Delta\bar{\tau}$ on the slip band. Slip band length represents distance along the slip band between grain boundaries in a single grain. Other material constants (shear modulus G specific fracture energy per unit area W_c, Poisson's ratio ν and frictional stress of dislocations on the slip plane, i.e. CRSS) can be found in the specialized literature[23] or calculated by means of MD (CRSS). According to Nakai,[38] the initiation conditions of small fatigue cracks still have not been clarified enough, because no method for successive, direct and quantitative observation of the process had been devised. In the presented model, cracks nucleate sequentially but on the segmental level. In each simulating iteration, just one segment of a particular grain is broken. It means that in one iteration, a segment belonging to one grain brakes, while in the following iteration, a segment of some other grain can break. In the presented case, the number of segments in each individual grain is equal to four. The total number of stress cycles N_{ini} needed for the initiation of a small crack is calculated by summing the cycles spent

to nucleate all cracks, including those coalesced to form the final small crack.

Jezernik *et al.*[24] used the Tanaka–Mura model to numerically simulate the small crack formation process. Three improvements were added to this model: (a) multiple slip bands inside each crystal grain as potential sites for crack nucleation, (b) crack coalescence between two grains and (c) segmented crack generation inside one grain. A numerical model was directed at simulating fatigue properties of thermally cut steel. The authors took into account accompanying residual stresses in order to simulate the properties of the thermally cut edge as faithfully as possible. As residual stresses are not taken into account in the original Tanaka–Mura model according to Eq. (3), in the present study, they are imposed as additional external loading. The superpositioning principle in linear elastic micromechanics analysis has been applied by taking residual stresses as part of the total load into account, which leads to the shear stress distribution shown in Fig. 4. Therefore, the residual stresses are implicitly evaluated in the Tanaka–Mura equation through the average shear stress range on the slip band $\Delta\bar{\tau}$.

Figure 4 shows the shear stress distribution and nucleated cracks for a typical high-cycle fatigue regime load level (450 MPa). In the beginning, cracks tended to occur scattered in the model and form in larger grains that are favourably oriented and show higher shear stresses. But after a while, existing single grain cracks started coalescing, causing local stress concentrations and amplifying the likelihood of new cracks forming near already coalesced cracks. When calculating cycles required for crack initiation, no cycles were attributed to crack coalescences (it is simulated as being instantaneous). The total number of cycles of crack initiation equals the sum of cycles needed for each microcrack to nucleate.

When the crack depth is less than a critical value, the crack growth behaviour has been found to be highly dependent upon the microstructure.[39–41] With increasing length, the growing cracks leave the originally 45° oriented slip planes and tend to propagate perpendicular to the external stress axis. The change of the crack plane from the active slip plane to a non-crystallographic plane perpendicular to the stress axis is called the transition from stage I (crystallographic propagation) to stage II (non-crystallographic propagation) or transition from crack initiation to crack propagation. In stage II of fatigue-crack propagation, only one crack usually propagates while most of other cracks usually stop within stage I.[15] Stage II of fatigue-crack propagation is simulated by using the power law crack propagation models based on the linear elastic fracture mechanics (LEFM).

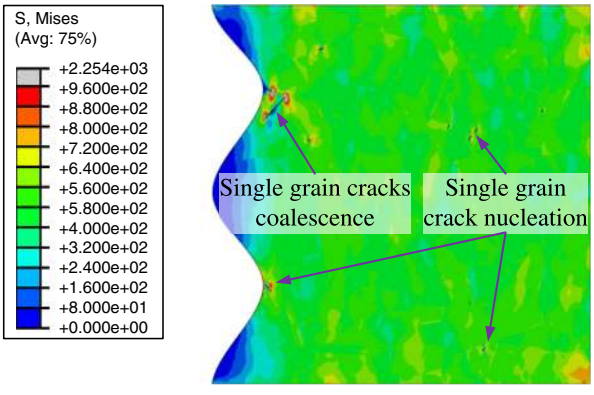

Fig. 4 Microcrack nucleation and subsequent coalescence.[24]

MODELLING AND SIMULATION OF CRACK PROPAGATION IN WELDED STIFFENED PANELS

It is well known that the residual stress in a welded stiffened panel is tensile along a welded stiffener and compressive in between the stiffeners. Residual stresses may significantly influence the SIF values and fatigue crack growth rate. A total SIF value, K_{tot}, is contributed by the part due to the applied load, K_{appl}, and by the part due to weld residual stresses, K_{res}, as given by Eq. (4):

$$K_{tot} = K_{appl} + K_{res}. \tag{4}$$

The so-called residual SIF, K_{res}, is required in the prediction of fatigue crack growth rates. The considered analysis method is based on the superposition rule of LEFM. The finite element method (FEM) has been widely employed for calculating SIFs. In the FE software package ANSYS,[32] the command INISTATE is used for defining the initial stress conditions. For evaluating K_{res}, it is important to input correct initial stress conditions to numerical models in order to characterize residual stresses.[28,42]

The effective SIF range ΔK_{eff} was considered in crack growth models in order to take crack closure effects on fatigue crack growth rate into account. The Elber[30] and Donahue[31] crack growth models are employed to simulate fatigue lifetime for welded stiffened panel specimens. In the Donahue model, the effective SIF range values are calculated on the basis of the applied load, without taking welding residual stresses into account. The Elber model takes into account both the applied load and the welding residual stresses, and the effective SIF range values are calculated on the basis of the effective SIF ratio R_{eff}, which depends on the $K_{tot,max}$ and $K_{tot,min}$ values. It is important to determine the total SIF values K_{tot} accurately, to model effects of residual stresses on crack propagation rate.

Specimen's geometry and loading conditions

Fatigue tests with constant stress range and frequency were carried out on a stiffened panel specimen with a central crack.[29] The specimen geometry is shown in Fig. 5. The material properties and chemical composition of the used mild steel for welding are given in Table 1.[43]

Table 2 shows the fatigue test conditions applied in the experiment. The cross-sectional area of the intact section and the average stress range away from the notch are denoted as A_0 and $\Delta\sigma$, respectively. The force range and the stress ratio are denoted by $\Delta F = F_{max} - F_{min}$ and $R = F_{min}/F_{max}$, respectively. The applied stress range was $\Delta\sigma = 80$ MPa. The initial notch length was $2a = 8$ mm, and the loading frequency was 3 Hz.

In the experiment, the crack lengths were measured by using the so-called crack gauges. The crack gauges are bonded to a specimen's surface in front of a crack tip in order to measure the length of a growing crack with respect to applied number of loading cycles. Different from usual strain gauges, the grid of crack gauges is cut along with crack development, resulting in resistance change.

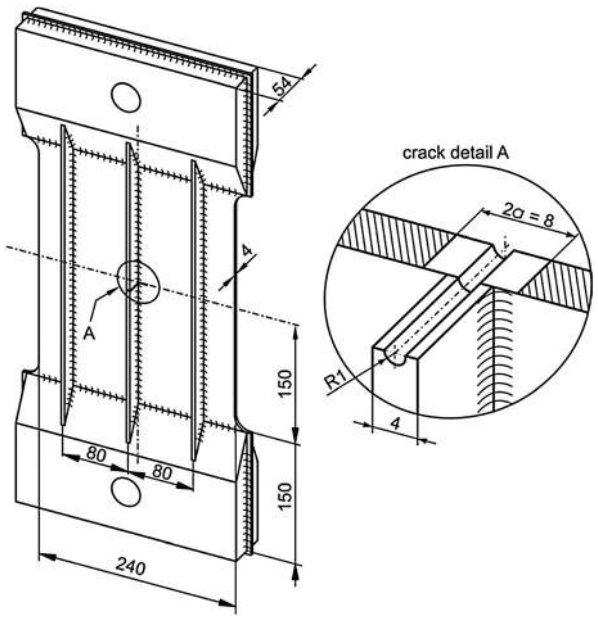

Fig. 5 Stiffened panel specimen.

Modelling of welding residual stresses in a stiffened panel by using finite element method

The residual stress distribution implemented in the present simulations follows Faulkner's model[44] in which the tensile regions around the stiffeners are modelled as rectangular shapes with a base width proportional to the plate thickness. For ship structures, the rectangular width typically ranges from 3.5 to 4 times the plate thickness. Dexter *et al.*[27] performed fatigue tests on half-scale welded stiffened panel specimens that model a part of a ship deck structure. The authors measured welding residual stresses in stiffened panel specimens and observed that the measured stresses vary mostly between a rectangular shape and a triangular shape.[27,28] Subsequent crack growth simulations showed that the residual stress distribution can be well described by a rectangular shape, where the maximum tensile stress equals to the yield stress of the considered material and compressive stresses between the stiffeners provide the equilibrium of internal forces.[28]

In this study, the distribution of welding residual stresses in the stiffened panel specimen is taken into account in a similar manner as in the model developed by Mahmoud and Dexter.[28] Residual stress distribution depicted in Fig. 6 was utilized for the considered specimen. This model presents the tensile regions around the stiffeners as rectangular shapes with a base width equal to 10 mm and with a stress level equal to yield strength $\sigma_0 = 235$ MPa. Estimated base width is in good agreement with Dexter's model,[28] where approximately one fourth of the span between the two stiffeners is exposed to tension. Compared with Faulkner's model, the base width used in this study is slightly shorter. The compressive residual stresses between the stiffeners and on the stiffeners were applied in the model to satisfy equilibrium.

To evaluate the SIF value contributed by the residual stresses, K_{res}, it is important to input correct initial stress conditions in the numerical model. Experimental measurements[27,28] showed that the profiles of welding residual stresses are almost identical along the axis parallel to the weld line. Correspondingly, in the FE model, elements with the same horizontal coordinate should have the same initial stress condition. For that purpose, a regular 1 mm size FE mesh was used, so that elements can be selected

Table 1 Material properties

Mechanical properties				
E – Young's modulus 206 000 MPa		ν – Poisson's coefficient 0.3		σ_0 – Yield strength 235 MPa
Chemical composition (%)				
C_{max} 0.18	Si_{max} 0.35	Mn_{min} 0.70	P_{max} 0.035	S_{max} 0.035

Table 2 Fatigue test conditions

A_0 (mm^2)	ΔF (N)	$\Delta\sigma$ (MPa)	R
1200	96000	80	0.0204

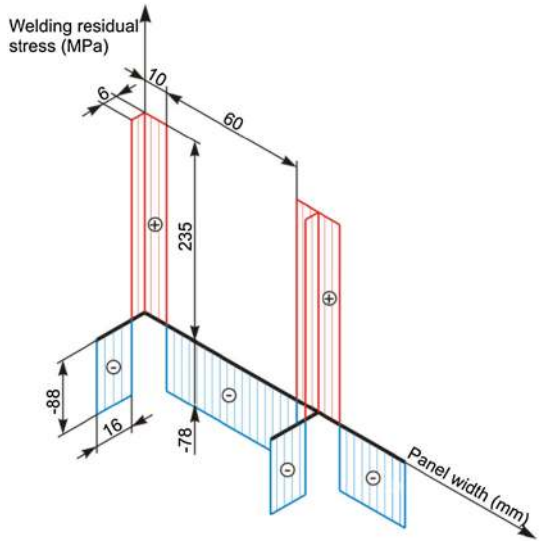

Fig. 6 Welding residual stress distribution.

in columns and associated with the corresponding initial stress level as given in Fig. 6. Applying initial stresses for the used eight-node shell elements is based on the element integration point. These initial stresses are equilibrated in the first analysis step. Because of the symmetry of specimen's geometry and loading conditions, it was sufficient to model only one quarter of the specimen. In ANSYS software package, the command INISTATE was implemented to define assumed initial stress conditions.[32] Figure 7 shows the σ_y component of the welding residual stresses in the stiffened panel specimen obtained for the implemented stress distribution as given in Fig. 6 (the σ_y stress component acts parallel to the loading axis).

Stress intensity factors and fatigue crack growth rate

For evaluating SIFs by FEM, the crack tip displacements extrapolation method was implemented.[32] The SIFs were determined in a linear elastic FE analysis. In the FE modelling, the crack tip region was meshed by singular elements. The procedure for the calculation of SIFs is based on the application of well-known 'quarter-point' elements introduced by Barsoum[45] and Henshell and Shaw.[46]

The near crack tip displacements and stresses of LEFM are usually related to the three fundamental deformation modes of fracture where mode I is the opening mode, mode II is the shearing mode and mode III is the tearing mode.[25,32] Opening displacement v in the vicinity of the crack tip, as depicted in Fig. 8, is given by Eq. (5).

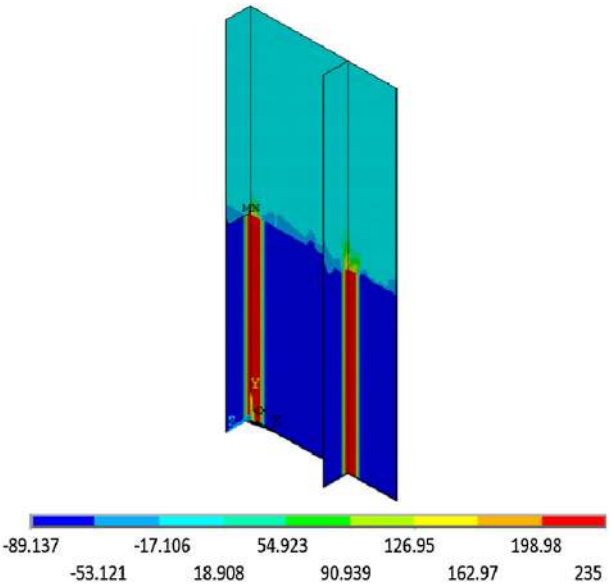

Fig. 7 Welding residual stresses in the stiffened panel specimen.

$$v = \frac{K_I}{4G}\sqrt{\frac{r}{2\pi}}\left[(2\kappa+1)\sin\frac{\theta}{2} - \sin\frac{3\theta}{2}\right] + \frac{K_{II}}{4G}\sqrt{\frac{r}{2\pi}}\left[(2\kappa-3)\cos\frac{\theta}{2} + \cos\frac{3\theta}{2}\right], \quad (5)$$

where K_I and K_{II} are the SIFs associated with modes I and II, G is the shear modulus, υ is the Poisson's ratio, v is the displacement in loading direction, and r and Θ are local polar coordinates. The conversion factor κ for plain stress conditions is given by Eq. (6).

$$\kappa = (3-\upsilon)/(1+\upsilon). \quad (6)$$

In Eq. (5), the higher-order terms are neglected, and the equation is therefore only valid in the vicinity of the crack tip. It should be noted that stress distribution is singular for $r = 0$. When Eq. (5) is applied to the half crack configuration illustrated in Fig. 8, the displacements v, across the faces of the crack are given by Eq. (7).

$$v = \frac{K_I}{2G}\sqrt{\frac{r}{2\pi}}(1+\kappa). \quad (7)$$

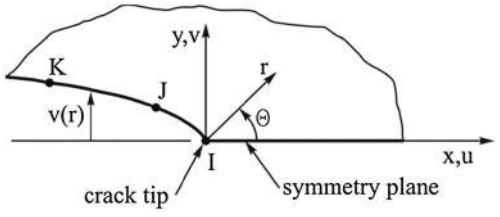

Fig. 8 Crack opening profile for a half crack model.

In the next step, we describe how K is obtained by using FE results and the theoretical equations given earlier. Attention is restricted to calculating the K_I factor for mode I displacements. The displacement v on the crack face of the half crack configuration depicted in Fig. 8 can be approximated by

$$v/\sqrt{r} = A + Br, \tag{8}$$

where A and B are constants determined from a linear curve fit of nodal displacements. Once A and B are determined, the limit $r \to 0$ is taken.

$$\lim_{r\to 0} \left(v/\sqrt{r}\right) = A \tag{9}$$

By combining Eqs (7) and (9) for the half crack model, the SIF is obtained as

$$K_I = \frac{2G\sqrt{2\pi}A}{(1+\kappa)}, \tag{10}$$

On the basis of the previously described technique, in the general post-processing procedure, the KCALC command was used to calculate the SIFs. The mode I SIF values, K_I, are determined for a stiffened panel specimen for a loading stress range $\Delta\sigma = 80$ MPa, assuming the presence of residual stresses as described earlier. The SIF values with respect to half crack length a are given in Fig. 9. K_{appl} represents the SIF values due to the applied stress range only, without residual stresses. K_{tot} represents the SIF values for the case when the residual stresses are taken into account along with the external loading stress range. It can be seen that residual stresses significantly increase K_{tot} values for shorter crack lengths, where tensile residual stresses prevail. Between the stiffeners, residual stresses reduce the K_{tot} values.

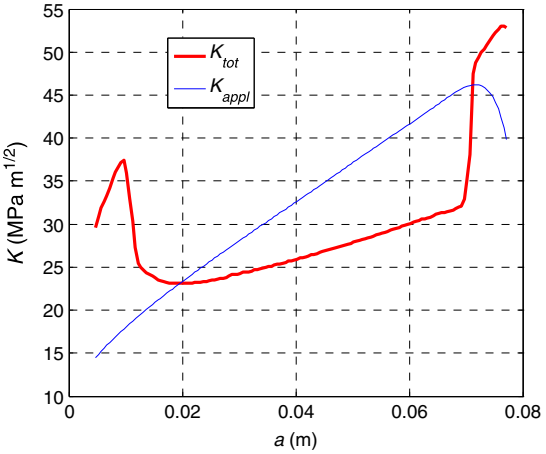

Fig. 9 K_{tot} and K_{appl} values.

A well-known method for predicting fatigue crack propagation under constant stress range is the power law (11) introduced by Paris and Erdogan.[26] In Eq. (11), da/dN and ΔK represent the crack growth rate and the SIF range, respectively. C and m are material constants, which are determined experimentally.

$$\frac{da}{dN} = C(\Delta K)^m \tag{11}$$

Elber[30] and Donahue *et al.*[31] further developed Paris' law assuming an effective SIF range, ΔK_{eff}, as the crack growth driving force parameter. Donahue *et al.*[31] defined the effective SIF range as $\Delta K_{eff} = K_{max} - K_{th}$, where K_{max} is the maximum SIF value in a loading cycle and K_{th} is an SIF threshold value below which no crack propagation occurs. Božić *et al.*[47,48] used this model to analyse fatigue crack propagation in plates damaged with single and multiple cracks, respectively. Assuming the stress ratio $R = 0$ as applied in the experiment, the threshold SIF value for the used mild steel was taken as $K_{th} = 6.8$ MPa.[49] The Donahue model predicted well fatigue lifetime and crack growth rate for centrally cracked un-stiffened plate specimens without welds and with a constant stress ratio $R = 0$.[47,48] However, this model does not take into account variable stress ratio R, which occurs in welded specimens due to residual stresses and can significantly influence the fatigue crack growth rate.

Elber[30] observed that crack closure decreases the fatigue crack growth rate by reducing the effective SIF range. He proposed an equation for the effective SIF range, which takes the load ratio R into account:

$$\Delta K_{eff} = (0.5 + 0.4R)\Delta K_{appl}. \tag{12}$$

In the present study, the nominal ratio R in Eq. (12) was replaced by the effective SIF ratio R_{eff}, in order to take into account the influence of welding residual stresses on fatigue crack propagation rate. The effective SIF ratio R_{eff} is defined as follows:

$$R_{eff} = \frac{K_{tot,min}}{K_{tot,max}} = \frac{K_{appl,min} + K_{res}}{K_{appl,max} + K_{res}}. \tag{13}$$

This superposition method based on the principle of LEFM was originally proposed by Glinka[50] and was

Table 3 Material's constants[a]

Model	C	m
Donahue	6.50×10^{-11}	2.75
Elber	1.67×10^{-10}	2.75

[a]The units for ΔK and $\Delta a/\Delta N$ are MPa $\cdot$ m$^{1/2}$ and m, respectively.

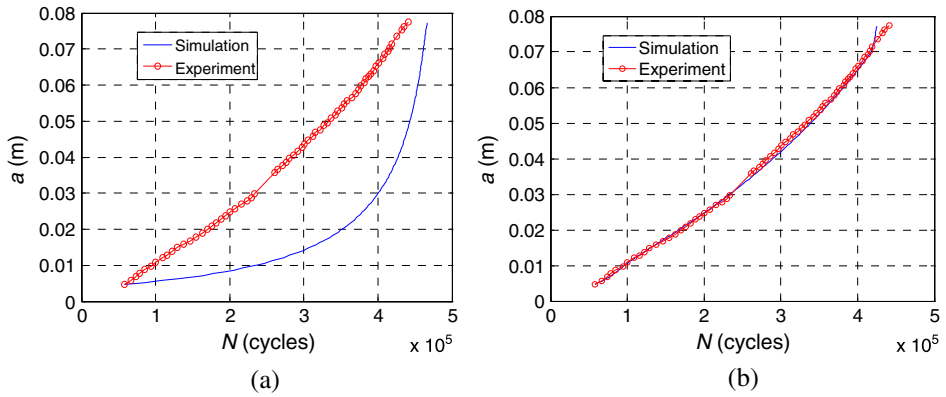

Fig. 10 Fatigue crack growth life for the applied stress range $\Delta\sigma_0 = 80$ MPa: (a) without residual stresses and (b) including residual stresses.

recently implemented in the FE modelling of fatigue crack growth rate in welded butt joints by Servetti and Zhang.[51] As the crack propagates under cyclic loading, the effective SIF ratio R_{eff} changes due to the presence of residual stresses.

The number of constant amplitude loading cycles due to which a crack propagates from its initial crack length, a_0, to a final crack length, a_{fin}, can be determined by the integration of Eq. (11), which becomes the following:

$$N = \int_{a_0}^{a_{fin}} \frac{\mathrm{d}a}{C\left[\Delta K_{eff}\right]^m}. \tag{14}$$

The integration of Eq. (14) can be performed numerically. Fatigue life was simulated for the specimen by integrating Eq. (14), where the material constants C and m were as given in Table 3. The exponent m for the considered material was determined in a previous study by means of crack growth rate diagrams based on a–N data obtained for centrally cracked plate specimens.[47] The C constants from Table 3 were estimated in a way to provide a good agreement of simulated fatigue lifetime with experimentally obtained a–N curve.

The Donahue model was implemented to the welded stiffened panel specimen, considering the effective SIF range values due to applied load only, $\Delta K_{eff} = K_{appl} - K_{th}$, without taking into account residual stresses. The Elber model takes into account the influence of residual stresses on fatigue crack growth rate by using the effective SIF range defined by Eq. (12) and the effective SIF ratio R_{eff} given by Eq. (13). For the two cases considered, the fatigue crack propagation life was obtained as shown in Fig. 10a and b. The presented measured crack lengths a are to be considered as averaged half crack lengths. These values are obtained by averaging measured crack lengths of the two propagating crack tips with respect to applied number of cycles N. The averaged half crack lengths are used in order to be comparable with the simulation results for semi-crack lengths obtained by the FE model where only one quarter of the specimen was modelled.

The FE analysis for the stiffened panel specimens showed that high tensile residual stresses in the vicinity of a stiffener significantly increase K_{res} and K_{tot}, as shown in Fig. 9. Correspondingly, the simulated crack growth rate was higher in this region, which is in good agreement with experimental results, as can be seen in Fig. 10b. Compressive weld residual stresses decreased the total SIF value K_{tot}. The Donahue model, which does not take account of welding residual stresses, could not simulate high crack growth rates in the vicinity of the stiffener, as can be seen in Fig. 10a. Fatigue crack growth simulation based on the Elber model, which takes into account the welding residual stresses, provides thus better agreement with experimental results in terms of crack growth rate and total number of cycles. In conclusion, residual stresses in welded stiffened panels should be taken into account for a proper evaluation of SIFs and fatigue crack growth rates.

In further work, one should do microstructural analyses in experiment and simulation (microscale and nanoscale) in order to foster the multiscale procedure and use the method to predict materials with improved fatigue properties in the future.

CONCLUSIONS

Simulation of cyclic loading to model dislocation nucleation as an initial step in fatigue initiation is possible in MD. Already after the very few cycles, essential changes in the system behaviour were observed under respective loading conditions. Contrary to the first cycles, where reversible changes were dominant, not dissolving restructuring occurs in the sense of dislocations and remaining lattice defects or, in other words, plasticity.

Numerical simulations of the fatigue crack initiation and growth of martensitic steel, based on a modified

Tanaka–Mura model, were presented. A simulation model related to the microcrack nucleation along slip bands was presented. Results obtained by using the proposed simulation model were compared to high cyclic fatigue tests and showed reasonably good agreement.

Crack propagation simulation based on numerical integration of a power law equation, taking account of welding residual stresses, was implemented to welded stiffened panel specimens. The FE analysis of the stiffened panel specimens showed that high tensile residual stresses in the vicinity of a stiffener significantly increase K_{res} and K_{tot}. The simulated crack growth rate was higher in this region, which is in good agreement with experimental results. Compressive welding residual stresses decreased the total SIF value K_{tot} and the crack growth rate between the two stiffeners. Residual stresses should thus be taken into account for a proper evaluation of SIFs and fatigue crack growth rates in welded stiffened panels.

Acknowledgements

This work was supported by the Deutsche Forschungsgemeinschaft (DFG) under Grant No. Schm 746/132-1 and as part of the Collaborative Research Centre SFB 716 at the University of Stuttgart, and by the Croatian Science Foundation Grant No. 120-0362321-2198. The support is gratefully acknowledged.

REFERENCES

1 Luo, C., Chattopadhyay, A. (2011) Prediction of fatigue crack initial stage based on a multiscale damage criterion. *Int. J. Fatigue*, **33**, 403–413.
2 Curtin, W. A., Deshpande, V. S., Needleman, A., Van der Giessen, E., Wallin, M. (2010) Hybrid discrete dislocation models for fatigue crack growth. *Int. J. Fatigue*, **32**, 1511–1520.
3 White, P. (2012). Molecular dynamic modelling of fatigue crack growth in aluminium using LEFM boundary conditions. *Int. J. Fatigue*, **44**, 141–150.
4 Horstemeyer, M. F., Farkas, D., Kim, S., Tang, T., Potirniche, G. (2010) Nanostructurally small cracks (NSC): a review on atomistic modeling of fatigue. *Int. J. Fatigue*, **32**, 1473–1502.
5 Božić, Ž., Schmauder, S., Mlikota, M., Hummel, M. (2013) Fatigue crack growth modelling in welded stiffened panels under cyclic tension, *13th International Conference on Fracture*, Beijing, China.
6 Stadler, J., Mikulla, R., Trebin, H. R. (1997) IMD: a software package for molecular dynamics studies on parallel computers. *Int. J. Mod. Phys.*, **8**, 1131–1140.
7 Bonny, G., Pasianot, R. C., Castin, N., Malerba, L. (2009) Ternary Fe-Cu-Ni many-body potential to model reactor pressure vessel steels: first validation by simulated thermal annealing. *Phil. Mag.*, **89**, 3531–3546.
8 Grottel, S., Reina, G., Dachsbacher, C., Ertl, T. (2010) Coherent culling and shading for large molecular dynamics visualization. *Comput. Graphics Forum Proc. of EUROVIS 2010*, **29**, 953–962.
9 Stukowski, A., Bulatov, V. V., Arsenlis, A. (2012) Automated identification and indexing of dislocations in crystal interfaces. *Modelling Simul. Mater. Sci. Eng.*, **20**, 85007–85023.
10 Stukowski, A. (2010) DXA user manual version 1.3.4. http://dxa.ovito.org/README.txt, (accessed in 04/22/2014).
11 Glodez, S., Jezernik, N., Kramberger, J., Lassen, T. (2010) Numerical modelling of fatigue crack initiation of martensitic steel. *Adv. Eng. Software*, **41**, 823–829.
12 Wood, W. A. (1956) Fatigue in Aircraft Structures, Academic Press, New York.
13 Fine, M. E., Ritchie, R. O. (1978) Fatigue-crack initiation and near-threshold crack growth. Fatigue and Microstructure. (Edited by M. Meshii), ASM, Metals Park (OH), pp. 245–278.
14 Laird, C. (1978) Mechanisms and theories of fatigue. Fatigue and Microstructure. (Edited by M. Meshii), ASM, Metals Park (OH), pp. 149–203.
15 Klesnil, M., Lukas, P. (1980) Fatigue of Metallic Materials, Elsevier, New York, pp. 57–80.
16 Mughrabi, H. (1988) Dislocation clustering and long-range internal stresses in monotonically and cyclically deformed metal. *Rev. Phys. Appl.*, **23**, 367–379.
17 Mughrabi, H. (2002) Fatigue: David L. Davidson symposium, *Warrendale* (*PA*): *TMS* (Edited by K. S. Chan, P. K. Liaw, R. S. Bellows, T. Zogas, W. O. Soboyejo, pp. 3–15.
18 Davidson, D. L., Chan, K.S. (1989) Crystallography of fatigue crack initiation in astrology at ambient temperature. *Acta Metall.*, **37**, 1089–1097.
19 Wang, Q. Y., Bathias, C., Kawagoishi, N., Chen, Q. (2002) Effect of inclusion on subsurface crack initiation and gigacycle fatigue strength. *Int. J. Fatigue*, **24**, 1269–1274.
20 Murakami, Y., Nomoto, T., Ueda, T. (2000) On the mechanism of fatigue failure in the superlong life regime ($N > 10^7$ cycles). Part 1: influence of hydrogen trapped by inclusions. *Fatigue Fract. Eng. Mater. Struct.*, **23**, 893–902.
21 Tanaka, K., Mura, T. (1981) A dislocation model for fatigue crack initiation. *J. Appl. Mech.*, **48**, 97–103.
22 Tanaka, K., Mura, T. (1982) A theory of fatigue crack initiation at inclusions. *Metall. Trans. A*, **13**, 117–123.
23 Brückner-Foit, A., Huang, X. (2006). Numerical simulation of micro-crack initiation of martensitic steel under fatigue loading. *Int. J. Fatigue*, **28**, 963–971.
24 Jezernik, N., Kramberger, J., Lassen, T., Glodez, S. (2010) Numerical modelling of fatigue crack initiation and growth of martensitic steels. *Fatigue Fract. Eng. Mater. Struct.*, **33**, 714–723.
25 Broek, D. (1989) The Practical Use of Fracture Mechanics. Kluwer Academic Publishers, Dordrecht, The Netherlands.
26 Paris, P., Erdogan, F. (1963) A critical analysis of crack propagation laws. *J. Basic*, **85**, 528–534.
27 Dexter, R. J., Pilarski, P. J., Mahmoud, H. N. (2003) Analysis of crack propagation in welded stiffened panels. *Int. J. Fatigue*, **25**, 1169–1174.
28 Mahmoud, H. N., Dexter, R. J. (2005) Propagation rate of large cracks in stiffened panels under tension loading. *Mar. struct.*, **18**, 265–288.
29 Sumi, Y., Božić, Ž., Iyama, H., Kawamura, Y. (1996) Multiple fatigue cracks propagating in a stiffened panel. *J. Soc. Naval Architects Japan* **179**, 407–412.
30 Elber, W. (1971) The significance of fatigue crack closure. *Damage tolerance in aircraft structures. ASTM STP 486. American Society for Testing & Materials*, 230–242.

31 Donahue, R. J., Clark, H. M., Atanmo, P., Kumble, R., McEvily, A. J. (1972) Crack opening displacement and the rate of fatigue crack growth. *Int. J. Fract.Mech.*, **8**, 209–219.

32 Swanson Analysis System, Inc. (2009) ANSYS user's manual revision 11.0.

33 Han, T., Luo, Y., Wang, C. (2014) Effects of temperature and strain rate on the mechanical properties of hexagonal boron nitride nanosheets. *J. Phys. D Appl. Phys.*, **47**, 025303–025311.

34 Tapasa, K., Bacon, D. J., Osetsky, Y. N. (2005) Simulation of dislocation glide in dilute Fe-Cu alloys. *Mater. Sci. Eng. A*, **400-401**, 109–113.

35 Kohler, C., Kizler, P., Schmauder, S. (2005) Atomistic simulation of precipitation hardening in α-iron: influence of precipitate shape and chemical composition. *Modell. Simul. Mater. Sci. Eng.*, **13**, 35–45.

36 Naveen Kumar, N., Durgaprasad, P. V., Dutta, B. K., Dey, G. K. (2012) Modeling of radiation hardening in ferritic/martensitic steel using multi-scale approach. *Comput. Mater. Sci.*, **53**, 258–267.

37 Latapie, A., Farkas, D. (2003) Molecular dynamics simulations of stress-induced phase transformations and grain nucleation at crack tips in Fe. *Modelling Simul. Mater. Sci. Eng.*, **11**, 745–753.

38 Nakai, Y. (2001) Evaluation of fatigue damage and fatigue crack initiation process by means of atomic-force microscopy. *Mater. Sci. Res. Int.*, **7**, 1–9.

39 Zabett, A., Plumtree, A. (1995) Microstructural effects on the small fatigue crack behaviour of an aluminum alloy plate. *Fatigue Fract. Eng. Mater. Struct.*, **18**, 801–809.

40 Taylor, D., Knott, J. F. (1981) Fatigue crack propagation behaviour of short cracks; the effect of microstructure. *Fatigue Fract. Eng. Mater. Struct.*, **4**, 147–155.

41 Miller, K. J. (1987) The behaviour of short fatigue cracks and their initiation: part II – a general summary. *Fatigue Fract. Eng. Mater. Struct.*, **10**, 93–113.

42 Bao, R., Zhang, X., Yahaya, N. A. (2010) Evaluating stress intensity factors due to weld residual stresses by the weight function and finite element methods. *Eng. Fract. Mech.*, **77**, 2550–2566.

43 Croatian Register of Shipping. (2012) Rules for the classification of ships. *Part 25 - Metallic Materials*.

44 Faulkner, D. (1975) A review of effective plating for use in the analysis of stiffened plating in bending and compression. *J Ship Res*, **19**, 1–17.

45 Barsoum, R.S. (1976) On the use of isoparametric finite elements in linear fracture mechanics. *Int. J. Numer. Methods Eng.*, **10**, 25–37.

46 Henshell, R. D., Shaw, K. G. (1975) Crack tip finite elements are unnecessary. *Int. J. Numer. Methods Eng.*, **9**, 495–507.

47 Božić, Ž., Mlikota, M., Schmauder, S. (2011) Application of the ΔK, ΔJ and ΔCTOD parameters in fatigue crack growth modelling. *Technical Gazette*, **18**, 459–466.

48 Božić, Ž., Schmauder, S., Mlikota, M. (2012) Fatigue growth models for multiple long cracks in plates under cyclic tension based on ΔK_I, ΔJ-integral and $\Delta CTOD$ parameter. *Key Eng. Mater.*, **488-489**, 525–528.

49 Liu, Y., Mahadevan, S. (2007) Threshold stress intensity factor and crack growth rate prediction under mixed-mode loading. *Eng. Fract. Mech.*, **74**, 332–345.

50 Glinka, G. (1979) Effect of residual stresses on fatigue crack growth in steel weldments under constant and variable amplitude load. *Fracture mechanics*, *ASTM STP 677*, *American Society for Testing and Materials*, 198–214.

51 Servetti, G., Zhang, X. (2009) Predicting fatigue crack growth rate in a welded butt joint: the role of effective R ratio in accounting for residual stress effect. *Eng. Fract. Mech.*, **76**, 1589–1602.